Chemomechanical Coupling and Motor Cycles of Myosin V

Veronika Bierbaum and Reinhard Lipowsky*
Theory and Bio-Systems, Max Planck Institute of Colloids and Interfaces, Potsdam, Germany

ABSTRACT The molecular motor myosin V has been studied extensively both in bulk and single molecule experiments. Based on the chemical states of the motor, we construct a systematic network theory that includes experimental observations about the stepping behavior of myosin V. We utilize constraints arising from nonequilibrium thermodynamics to determine motor parameters and demonstrate that the motor behavior is governed by three chemomechanical motor cycles. The competition between these cycles can be understood via the influence of external load forces onto the chemical transition rates for the binding of adenosine triphosphate and adenosine diphosphate. In addition, we also investigate the functional dependence of the mechanical stepping rates on these forces. For substall forces, the dominant pathway of the motor network is profoundly different from the one for superstall forces, which leads to a stepping behavior that is in agreement with the experimental observations. Our theory provides a unified description of the experimental data as obtained for myosin V in single motor experiments.

INTRODUCTION

Myosin V is a processive molecular motor that moves along actin filaments in discrete steps of 36 nm (1). This processive motion is tightly coupled to the hydrolysis of adenosine triphosphate (ATP) (2). The molecule has a catalytic domain at each of its two heads and proceeds in a hand-over-hand fashion toward the barbed end of the actin filament (3). The coordination of hydrolysis between the two heads is thought to be crucial for the processive motion and the high duty ratio of the motor (4,5). For external forces opposing the forward motion of the motor that do not exceed its stall force, i.e., the force at which the motor does not exhibit any net motion, a dominant chemomechanical cycle has been identified.

The molecule mainly dwells with both heads strongly bound to the filament, with adenosine diphosphate (ADP) bound to both catalytic domains. After release of ADP from the trailing head, ATP binding to the empty domain takes place. This leads to weakening of the actomyosin bond, which in turn allows for unbinding of the head from the actin filament. Subsequently, the free head finds its way to the next binding site via a power stroke, and a subsequent diffusional search until encounter with the next binding site (6), where it rebinds and hydrolyzes the ATP molecule (5) to a ADP*P complex with subsequent release of P (phosphate). At high concentrations of ATP, the release of ADP is the rate-limiting step of this turnover cycle.

Extensive research has been done on the step-size distribution of the molecule (1), its dwell times (7), and its backstepping behavior (8). Moreover, the release of ADP has been proposed to be different for the leading and the trailing head of the molecule (9,10). Reported data on the stall force range from 1.5 to 3.0 pN for various concentrations of ATP (1,8,11–13). Three different force regimes have to be distinguished: Assisting forces as well as resisting forces below and above the stall force F_s of the motor. For resisting forces that exceed stall, myosin V has been proposed to act as a mechanical ratchet (13): When stepping backward in a forced manner, the stepping velocity does not seem to depend on the concentration of ATP, whereas this is not the case for the forward motion of the motor under assisting forces.

A variety of theoretical models has been proposed for myosin V, such as a kinetic model (14), and a treatment of the molecule implementing the elastic properties of its lever arms (15). A stochastic algorithm for the fit of dwell time distributions has been proposed by Liao et al. (16), and the molecule serves as a model mechanism to evaluate its properties in terms of efficiency (17). A recent study (18) performs a Brownian dynamics simulation of the forward motion of myosin V, with the aim to investigate the substepping behavior that has been reported by different groups (11,19). A generic class of discrete models addresses the substepping behavior (20) and the reaction of enzymatic activity to high forces (21). The models, however, are either based on a large number of parameters or do not address the force dependence of the myosin V stepping behavior. In addition, none of them investigates the role of backward steps quantitatively, especially the step ratio and the ratcheting behavior of myosin V.

Here, we use a network representation deduced from the enzymatic activity of the myosin motor to explain several sets of experimental data, including those on backward steps. Our approach is based on previous work (22,23) that provides a general framework for the chemomechanical coupling of molecular motors which is consistent with nonequilibrium thermodynamics.

Our article is organized as follows. In Methods, we describe our network representation, the theoretical description of the motor dynamics, as well as the balance conditions for the motor cycles. In Results, we discuss the force dependence of the transition rates over the whole range of load forces. In addition, we use thermodynamic constraints

Submitted October 1, 2010, and accepted for publication February 8, 2011.

*Correspondence: lipowsky@mpikg.mpg.de

Editor: R. Dean Astumian.

0006-3495/11/04/1747/9 $2.00

doi: 10.1016/j.bpj.2011.02.012

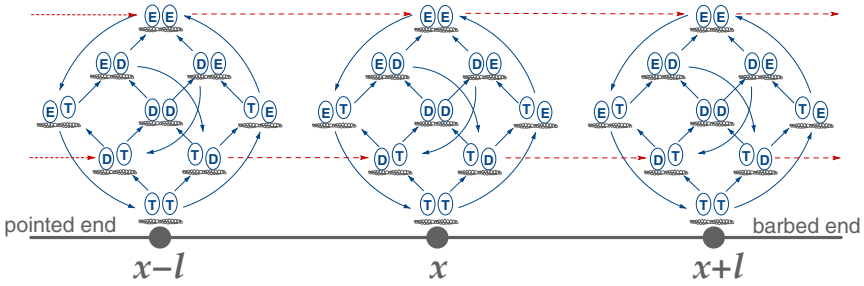

FIGURE 1 Chemomechanical network for myosin V at different binding sites x of the filament, represented by a thick gray line. The nine states, that are repeated periodically along the filament with a spacing of $\ell = 36$ nm, are defined by the chemical composition of the nucleotide-binding pockets of the two motor heads. A head with bound ATP or ADP is denoted by T or D, an empty head by E. Both the E and D states are strongly bound to the actin filament, whereas the T state is only weakly attached (24), as indicated by the gap between the T heads and the filament. All transitions between two connected states can occur in both forward and backward direction. Chemical transitions are drawn as solid lines (*blue*), with arrows indicating the direction of ATP hydrolysis. The broken lines (*red*) correspond to the mechanical transitions as observed experimentally, with the arrows pointing toward the forward stepping direction (13,19), i.e., toward the barbed-end of the actin filament.

to determine those parameters of our network that are not accessible to experiments. We show that the ratcheting behavior of myosin V can be explained by different chemomechanical cycles that are dominant for different force regimes. We calculate the velocity, step ratio, and run-length of the motor as a function of load force and nucleotide dependence and compare these quantities with experimental findings. Finally, we summarize our results in Discussion and Concluding Remarks.

METHODS

Network representations

During processive motion, the motor can attain several states, specified by its location on the motor filament and the chemical composition of its nucleotide-binding pockets. The transitions between these states involve binding or release of ATP, ADP, or P, or a mechanical displacement. For the definition of discrete motor states that separate the chemical reaction from the step, two requirements have to be fulfilled, 1), thermal equilibrium has to be reached on a timescale much shorter than the duration of the chemical reaction; and 2), the step in itself has to be much faster than the reaction. This is indeed the case for the myosin V molecule, for which the hydrolysis rate is ~10/s and the mechanical step takes only a few milliseconds to be completed (19,24,25).

A single catalytic domain of the motor can contain bound ATP, ADP, or ADP*P, or it can be empty. When combining the ADP*P state with the transition between the ATP and the ADP state, as discussed in Lipowsky et al. (22), each of the two catalytic sites of the motor can attain three states that we denote by T (ATP bound), D (ADP bound), and E (empty). This state space for a single motor head leads to $3 \times 3 = 9$ possible states for the two heads. These 9 states are connected by 18 chemical reactions and 6 mechanical displacements, each of which can occur in the forward and backward direction. A chemical transition corresponds to a chemical forward or backward reaction and involves the binding or release of a nucleotide, whereas a mechanical transition results in the swapping of the two motor heads. In general, the possible mechanical transitions are, without specification of the step direction,

$$\mathrm{EE} \rightleftharpoons \mathrm{EE},\ \mathrm{DD} \rightleftharpoons \mathrm{DD},\ \mathrm{TT} \rightleftharpoons \mathrm{TT},\ \mathrm{ET} \rightleftharpoons \mathrm{TE},$$

$$\mathrm{DT} \rightleftharpoons \mathrm{TD},\ \text{and}\ \mathrm{DE} \rightleftharpoons \mathrm{ED}.$$

In Fig. 1, the chemical network of myosin V is repeated with periodic boundary conditions along a filament coordinate x with a discrete spacing of $\ell = 36$ nm. The chemical transitions connect the nine states of the network, whereas the mechanical transitions connect two copies of the network separated by a step of size ℓ. Only those two mechanical transitions are included that have been observed in experiments, namely

$$\mathrm{EE} \rightleftharpoons \mathrm{EE},\ \text{and}\ \mathrm{TD} \rightleftharpoons \mathrm{DT}.$$

The network shown in Fig. 1 contains 36 chemical and 4 mechanical transitions which lead, in general, to a rather large number of possible pathways or motor cycles. In the following, we identify the dominant pathways of the motor and, in this way, reduce the network description. This procedure enables us to minimize the number of model parameters and to construct a theory which, on the one hand, describes a large set of experimental data as obtained by different groups and, on the other hand, can be improved if new experimental data become available.

The simplest chemomechanical network that takes both mechanical transitions TD $\rightleftharpoons$ DT and EE $\rightleftharpoons$ EE into account is displayed in Fig. 2. Apart from the two mechanical transitions, this network contains six chemical transitions, each of which may proceed in the forward or backward direction. As shown in the following, the available experimental data allow us to determine the corresponding transition rates for vanishing load force in a unique manner.

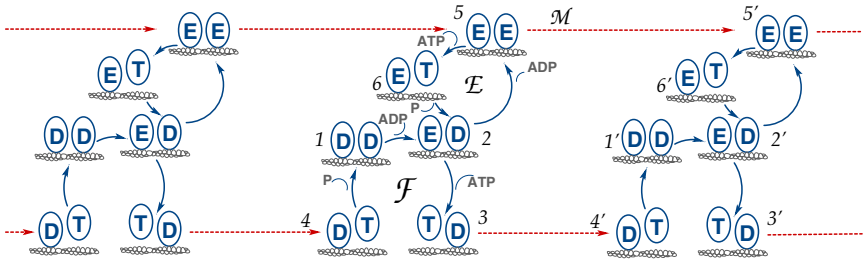

FIGURE 2 Reduced network for the motion of myosin V, consisting of three copies of six states $i = 1\ldots6$ connected by transitions $|ij\rangle$ from state i to state j, that form three pathways $\mathcal{F}$, $\mathcal{L}$, and $\mathcal{M}$. The chemomechanical forward cycle $\mathcal{F}$ consists of the states $\langle 1234' \rangle$, which contain both chemical and mechanical transitions, while the dissipative or enzymatic slip cycle $\mathcal{L}$ with states $\langle 256 \rangle$ is purely chemical. The ratcheting cycle $\mathcal{M}$, on the other hand, consists only of the mechanical stepping transitions $|55'\rangle$, $|5'5''\rangle$, and so on. Each state is characterized by the chemical composition of the two motor heads, the one on the right-hand side being the leading one. The solid lines (*blue*) are the chemical transitions for the indicated species $X =$ ATP, ADP, or P, while the broken lines (*red*) show the stepping transitions. The arrows refer to the direction of forward stepping and ATP hydrolysis, respectively.

With the use of periodic boundary conditions for the network, each state can be revisited on a closed path. A network cycle consists of a set of states that are directly connected and have, as a starting and end point, either the same state or the corresponding copy at a neighboring lattice site of the network. A cycle with a primed state indicates that it contains a mechanical displacement ℓ. The network thus can be characterized by three cycles $\mathcal{M}$, $\mathcal{E}$, and $\mathcal{F}$, two of which contain a stepping transition. Each of these cycles is composed of two directed cycles, i.e., the forward cycles,

$$\mathcal{F}^+ = |1234'\rangle,\ \mathcal{E}^+ = |256\rangle,\ \text{and}\ \mathcal{M}^+ = |55'\rangle,$$

and their corresponding backward cycles,

$$\mathcal{F}^- = |4'321\rangle,\ \mathcal{E}^- = |652\rangle,\ \text{and}\ \mathcal{M}^- = |5'5\rangle.$$

The chemomechanical cycle $\mathcal{F}$ (DD $\rightleftharpoons$ ED $\rightleftharpoons$ TD $\rightleftharpoons$ DT $\rightleftharpoons$ DD) is the one discussed previously in various experimental studies ((5,7), and see Section S1 in the Supporting Material), and contains both chemical and stepping transitions. The ratcheting cycle $\mathcal{M}$ contains only the stepping transition EE $\rightleftharpoons$ EE, corresponding to the experimental result in Gebhardt et al. (13) where myosin V was observed to step at superstall forces in the EE state. The third cycle, $\mathcal{E}$ (EE $\rightleftharpoons$ ET $\rightleftharpoons$ ED), is a dissipative cycle that connects the two stepping cycles $\mathcal{M}$ and $\mathcal{F}$ along two different pathways, one involving ATP hydrolysis and the other the binding of ADP.

Myosin V exhibits rather different stepping behavior for load forces below and above the stall force. Our analysis as described below shows that this difference arises from different cycles of the network being dominant for different force regimes. The chemomechanical cycle $\mathcal{F}$, which couples the mechanical forward steps TD $\rightarrow$ DT or $|34'\rangle$ to ATP hydrolysis, is dominant for forces below the stall force. In this regime, the motor also exhibits some backward steps DT $\rightarrow$ TD or $|4'3\rangle$, but these backward steps are immediately followed by forward steps. Thus, these backward steps are not coupled to ATP synthesis, a process that is rather unlikely for typical nucleotide concentrations. The mechanical slip cycle $\mathcal{M}$ dominates for forces above the stall force. In the latter regime, the motor walks backward in a processive manner. The stall force itself is determined by the competition between the chemomechanical cycle $\mathcal{F}$ and the mechanical slip cycle $\mathcal{M}$.

It is instructive to compare these operation modes of myosin V with those of kinesin. For the latter motor, the sub- and superstall regimes are governed by two different chemomechanical cycles, one of which couples mechanical backward steps to ATP hydrolysis (23). The latter coupling has also been discussed for myosin V (26). In the case of kinesin, the competition between the two chemomechanical cycles leads to a stall force that is essentially independent of ATP concentration (23), in agreement with single molecule data. In contrast, the experimentally determined values for the stall force of myosin V lie within a relatively broad range (1,8,11–13). Therefore, at present, the experimental data provide no evidence for the relevance of another chemomechanical cycle that couples backward steps of myosin V to ATP hydrolysis.

Motor dynamics

The transitions between two connected states of the network take place in a stochastic manner. Thus, the probability $P_i(t)$ to find the motor in state i at time t, evolves according to a master equation

$$\frac{\mathrm{d}}{\mathrm{d}t}P_i(t) = -\sum_j \Delta J_{ij}(t), \tag{1}$$

with

$$\Delta J_{ij}(t) \equiv P_i(t)\omega_{ij} - P_j(t)\omega_{ji} \tag{2}$$

being the local excess flux through the transition between two states i and j, where the transition rate ω_{ij} is given by the number of transitions from i to j per unit time. In general, the transition rates ω_{ij} can depend on both the load force component parallel to the filament, $F = \vec{F}_{\|}$, and the molar concentrations $[X]$, where X denotes the molecular species ATP, ADP, or P. Thus, the transition rates have the general form

$$\omega_{ij} \equiv \omega_{ij,0}\Phi_{ij}(F) \ \text{ with } \ \Phi_{ij}(0) \equiv 1, \tag{3}$$

which defines the zero-force transition rates $\omega_{ij,0}$ and the force-dependent factors $\Phi_{ij}(F)$. Moreover, the transitions that include binding of an X-molecule with X = ATP, ADP, and P depend on the molar concentration $[X]$, which implies

$$\begin{aligned} \omega_{ij,0} &\equiv \widehat{\kappa}_{ij}[X] \quad \text{for } X-\text{binding}, \\ &\equiv \kappa_{ij} \qquad \text{for } X-\text{release}. \end{aligned} \tag{4}$$

Note that the transition rate constants $\widehat{\kappa}_{ij}$ have the dimension 1/(s μM) whereas the transition rates κ_{ij} have the dimension 1/s. In the steady state, the probability distribution $P_i = P_i^{st}$ of the motor is independent of time, i.e., $dP_i^{st}/dt = 0$, and the dynamics of the system is determined by the corresponding steady-state fluxes $J^{st}{}_{ij}$. Every time the motor undergoes a stepping transition, it performs a step with length ℓ = 36 nm. The average velocity of the motor is thus given by

$$v = \ell\left(\Delta J^{st}_{34'} + \Delta J^{st}_{55'}\right), \tag{5}$$

i.e., by the combined flux through the two stepping transitions $|34'\rangle$ and $|55'\rangle$.

In Section S2 of the Supporting Material, we discuss the energetic balance of the motor, which can be specified in a quantitative manner in terms of network dicycles $\mathcal{C}^d_\nu$ where ν specifies the cycle and $d = \pm 1$ the orientation of the dicycle. Thus, it is convenient to consider cyclic fluxes rather than fluxes through single transitions. The excess flux along the dicycle $\mathcal{C}$ of the network has the form

$$\Delta J^{st}\left(\mathcal{C}^+\right) \equiv J^{st}\left(\mathcal{C}^+\right) - J^{st}\left(\mathcal{C}^-\right), \tag{6}$$

where $J^{st}(\mathcal{C}^\pm)$ are the dicycle fluxes in the positive (+) and negative (−) direction of the cycle, respectively. Any local excess current $\Delta J^{st}{}_{ij}$ can be written as a linear superposition of dicycle excess fluxes.

Force-dependence of transition rates

The force-dependence of the transition rates ω_{ij} is contained within the force-dependent factors $\Phi_{ij}(F)$ as defined by Eq. 3. These factors satisfy certain balance conditions as derived in Liepelt and Lipowsky (27) for arbitrary chemomechanical networks. (The corresponding conditions for myosin V are described in Section S2 in the Supporting Material; see also Eqs. S10–S13.) These conditions provide constraints on products of the ratios $\Phi_{ij}(F)/\Phi_{ji}(F)$ but do not determine the force-dependence of the individual factors. For the latter dependence, we use distinct functional forms for the mechanical and chemical rates as described in the following.

Mechanical transitions

The force dependence of the mechanical transitions within the cycle $\mathcal{F}$ is parameterized in the usual form (20,23) as

$$\Phi_{34'}(F) = \exp\left(-\theta_{ij}\frac{\ell}{k_\mathrm{B}T}F\right) \tag{7}$$

for the forward step $|34'\rangle$ and as

$$\Phi_{4'3}(F) = \exp\left(\left(1-\theta_{ij}\right)\frac{\ell}{k_\mathrm{B}T}F\right) \tag{8}$$

for the backward step $|4'3\rangle$ with $0<\theta_{ij}<1$.

The parameterization as given by Eqs. 7 and 8 is plausible if the force-induced deformation energy is small compared to the energy barrier that has

to be overcome to perform a step in the absence of force. However, this parameterization is not applicable to the limit of large forces. In particular, when the motor motion is governed by the mechanical cycle $\mathcal{M}$, the parameterization in Eqs. 7 and 8 would lead to an exponential increase of the stepping rate, which does not correspond to the experimental observation. Therefore, the force dependence of the stepping transitions $\omega_{55'}$ and $\omega_{5'5}$ within the mechanical ratchet cycle $\mathcal{M}$ is calculated from the escape of a particle over a potential barrier using an appropriate Fokker-Planck equation, as shown in Section S3 in the Supporting Material. The rates are then given by

$$\omega_{5'5} = \frac{D}{k_B T}\frac{F\ell - U_{ba}}{\ell^2}\frac{1}{1-\exp\left[\frac{1}{k_B T}(U_{ba}-F\ell)\right]} \quad (9)$$

and

$$\omega_{55'} = \exp\left(-\frac{\ell}{k_B T}F\right)\omega_{5'5}, \quad (10)$$

where U_{ba} is the height of the potential barrier and D is an apparent diffusion constant.

Chemical transitions

For the force-dependent factors $\Phi_{ij}(F)$ of the chemical rates, we use the parameterization

$$\Phi_{ij}(F) = \frac{1+\exp\left(-\chi_{ij}\frac{\ell}{k_B T}F'\right)}{1+\exp\left(\chi_{ij}\frac{\ell}{k_B T}(F-F')\right)}, \quad (11)$$

which involves the dimensionless parameter χ_{ij} and the characteristic force F'. The force-dependent factors Φ_{ij} as given by Eq. 11 satisfy $\Phi_{ij}(0) = 1$ as required by Eq. 3, fulfill the obvious conditions $0 \le \Phi_{ij}(F) \le \infty$ for all F, and decay to zero for large resisting loads $F > 0$. For $F' = 0$, the expression in Eq. 11 reduces to the force-dependent factors Φ_{ij} as previously used in Liepelt and Lipowsky (23) to describe the single motor data for kinesin. A nonzero value of F' as introduced here represents a threshold value for the load force F. Indeed, this load force needs to exceed the characteristic force F' to have an appreciable effect on the chemical transitions.

RESULTS

Specification of transition rates

For vanishing load $F = 0$, we use the ATP binding rates $\widehat{\kappa}_{23}$ and $\widehat{\kappa}_{56}$ as well as the phosphate release rates κ_{41} and κ_{62} as determined experimentally for single-headed myosin V in De La Cruz et al. (24). We also incorporate the previously mentioned gating mechanism which implies that the ADP release rate of the motor's leading head is smaller than the one of the trailing head (5,32). The reduced network considered here involves the transition $|12\rangle$ with ADP release from the trailing head and the transition $|25\rangle$ with ADP release from the leading head (see Fig. 2). Therefore, in our theory, the gating mechanism is incorporated via the transition rate ratio $\zeta \equiv \kappa_{25}/\kappa_{12}$. We find that average motor properties such as the motor velocity v, the ratio q of forward/backward steps, and the run-length Δx can be well described for ζ-values within the range $1/10 \lesssim \zeta \lesssim 1$, consistent with the experimental data in Purcell et al. (32). However, a detailed comparison of calculated and measured dwell time distributions (V. Bierbaum and R. Lipowsky, unpublished) leads to the specific choice $\zeta = 1/10$ as used here. In addition, we use the rates for ADP binding, $\widehat{\kappa}_{21}$ and $\widehat{\kappa}_{52}$, as measured in Rief et al. (7).

The remaining unknown chemical rates in the chemomechanical cycle $\mathcal{F}$ and the enzymatic slip cycle $\mathcal{E}$ are the ATP release rates, κ_{32} and κ_{65}, and the phosphate binding rates, $\widehat{\kappa}_{14}$ and $\widehat{\kappa}_{26}$. The rate of ATP release is rather small and thus difficult to measure (28). In the absence of experimental values for the ATP release rate of myosin V, we make the plausible assumption that this rate is of the same order of magnitude as the corresponding rate for myosin II. The latter rate has been determined experimentally and is $\sim 10^{-5}$ s^{-1} (29). It turns out that increasing this rate by up to three orders of magnitude does not significantly change our calculations, with the exception of the stepping velocity as a function of phosphate concentration, as discussed in the next section.

We use the zero-force balance condition (see Eq. S5 in the Supporting Material) to determine the phosphate binding rates $\widehat{\kappa}_{14}$ and $\widehat{\kappa}_{26}$ (as shown explicitly in Section S4 in the Supporting Material). The zero-force rates for the mechanical steps, $\kappa_{34'}$ and $\kappa_{4'3}$, describe the motor's tendency to move in the forward or backward direction, respectively. For the forward stepping rate $\kappa_{34'}$, we use a value deduced from simulations (18), and extract the backward stepping rate $\kappa_{4'3}$ by comparison of our calculations with the measurements in Kad et al. (8) using a procedure explained further below. Once the mechanical stepping rates have been determined, the phosphate binding rate $\widehat{\kappa}_{14}$ follows from the balance relation (see Eq. S19 in the Supporting Material).

The force dependence of the chemical transition rates is, in general, difficult to determine experimentally. In single-headed constructs of myosin V, the force dependence of the binding and dissociation rates of ADP has been investigated (10). For a single head, the ADP dissociation rate increases for assisting forces and decreases for resisting forces, and the ADP binding rate decreases for both forces. The implications of these latter observations for the behavior of double-headed myosin are not obvious, however, because internal strain may significantly influence the force exerted on the catalytic site of the molecule (5) and reduce this force dependence to some extent.

We found that the available single motor data can be described if only two chemical transition rates are taken to be force-dependent, namely the rates of the transitions $|56\rangle$ and $|52\rangle$ for ATP and ADP binding to the leading head. For these two transitions, we chose the parameterization as given by Eq. 11 with $F' = 1.6$ pN, comparable to the internal strain estimated in Veigel et al. (5), and

$$\chi_{56} = \chi_{52} = 4.$$

The latter equality is imposed by the balance condition (see Eq. S7 in the Supporting Material) because all other chemical transition rates are taken to be force-independent with

$\Phi_{ij}(F) \equiv 1$ (see Table S1). It is tempting to interpret the force-dependence of the rates for ATP and ADP binding to the leading head in terms of elastic deformations of the motor molecule. Indeed, if the motor is exposed to the load force F, the leading head should experience a larger elastic stress and, thus, a larger deformation compared to the trailing head. If this deformation induced a partial closure of the nucleotide-binding pocket of the leading head, binding of both ATP and ADP would be suppressed.

Motor velocity in the absence of load

The stepping velocity of the motor, given by Eq. 5, has the general form

$$v = v(F, [\mathrm{ATP}], [\mathrm{ADP}], [\mathrm{P}]), \tag{12}$$

i.e., it depends both on the load force F and on the nucleotide concentrations [ATP], [ADP], and [P]. For $F = 0$, the mechanical step cycle $\mathcal{M}$ does not contribute to the stepping velocity. In the limit of vanishing ADP and P, the stepping velocity arises predominantly through the chemomechanical cycle $\mathcal{F}^+$ and the enzymatic slip cycle $\mathcal{E}^+$, while the backward cycles $\mathcal{F}^-$ and $\mathcal{E}^-$ are suppressed. The competition between the two dicycles $\mathcal{F}^+$ and $\mathcal{E}^+$ is governed by the competition of the rates ω_{23} and ω_{25} corresponding to ATP binding by the trailing head and to ADP release from the leading head, respectively. For saturating values of [ATP], the ATP binding rate associated with $\mathcal{F}^+$ is large compared to the ADP release rate of $\mathcal{E}^+$, and the network can be reduced to the forward cycle $\mathcal{F}$ only. For this unicycle network, the velocity exhibits the Michaelis-Menten-like behavior as given by

$$\begin{aligned} v &= \ell \Delta J^{st}_{34'} \\ &= \frac{1}{\Omega}\kappa_{41}\kappa_{12}\widehat{\kappa}_{23}\kappa_{34'}\left([\mathrm{ATP}] - \frac{[\mathrm{ADP}][\mathrm{P}]}{K_{\mathrm{eq}}}\right) \approx \frac{v_{sat}[\mathrm{ATP}]}{K_M + [\mathrm{ATP}]}, \end{aligned} \tag{13}$$

with Ω being a normalization constant consisting of terms that are multilinear in [ATP], [ADP], and [P]. Here, K_M is the effective Michaelis constant and v_{sat} the saturation velocity for large ATP concentration, and the second asymptotic equality in Eq. 13 applies to the limit of small product concentrations, i.e., small [ADP] and [P]. The calculated values for v_{sat} and K_M are presented in Table 1, where we have used the transition rates specified in Table 2.

Using the complete network, we can also calculate the stepping velocity as a function of other control parameters. Fig. 3 shows the velocity dependence on one of the nucleotide concentrations [X] with X = ATP, ADP, or P in the absence of load, keeping the other two concentrations fixed. In general, the experimental choices for the fixed concentrations were taken to be low [ADP] and [P] and saturating [ATP] (see Fig. 3, *inset*). As can be inferred from Fig. 3, the calculated velocity dependence on [ATP] is in good agreement with the data. Moreover, our model captures the inhibiting effect of ADP on the stepping velocity, as measured in Baker et al. (12). Increasing the P concentration, with saturating [ATP] and low [ADP], inhibits the stepping velocity in a way that is comparable to the effect of ADP. This inhibition, however, is reduced for a higher value of the ATP release rate, which has been chosen here to be equal to the value of myosin II due to lack of experimental information. Increasing the ATP release rate leads to a decrease of the P binding rate as a consequence of the balance condition (see Eq. S5 in the Supporting Material), and thus to a weakening of the inhibition effect on the velocity.

TABLE 1 Comparison of saturating velocity v_{sat} and Michaelis constant K_M

	Experiment (Ref.)	Forward cycle $\mathcal{F}$
v_{sat}	400–500 nm/s (1,7,11,30,34)	412 nm/s
K_m	12 μM (7)	10.8 μM

As determined experimentally in the literature (1,7,11,30,34) and calculated via Eq. 13 for the reduced unicycle network that consists only of the forward cycle $\mathcal{F}$ in Fig. 2.

Motor velocity and step ratio in the presence of load

We now address the dependence of the motor's stepping velocity on force F, where we distinguish two force regimes, below and above the stall force F_s. For assisting forces and

TABLE 2 Transition rates for the motor network displayed in Fig. 2 for $F = 0$, i.e., in the absence of external load

Rate	$\kappa_{ij}, \widehat{\kappa}_{ij}$	Value	Ref.
ATP binding*	$\widehat{\kappa}_{23}, \widehat{\kappa}_{56}$	0.9 (μM s)$^{-1}$	(24)
ATP release†	κ_{32}, κ_{65}	2×10^{-5} s^{-1}	(29)
ADP binding*	$\widehat{\kappa}_{21}, \widehat{\kappa}_{52}$	4.5 (μM s)$^{-1}$	(7)
ADP release*	κ_{12}	12 s^{-1}	(24)
ADP release‡	κ_{25}	1.2 s^{-1}	—
P binding†	$\widehat{\kappa}_{14}$	0.65 (μM s)$^{-1}$	—
	$\widehat{\kappa}_{26}$	6×10^{-7} (μM s)$^{-1}$	—
P release*	κ_{41}, κ_{62}	250 s^{-1}	(24)
Step	$\kappa_{34'}$§	7000 s^{-1}	(18)
	$\kappa_{4'3}$‡	0.65 s^{-1}	—
	$\kappa_{55'}$‡, $\kappa_{5'5}$‡	1.5×10^{-8} s^{-1}	—

The experimental values in De La Cruz et al. (24) and Rief et al. (7) have been obtained for monomeric and dimeric myosin V, respectively. A significant discrepancy is found between these two myosins for the binding rate of ADP, which was estimated to be 10–12 (μM s)$^{-1}$ for monomeric myosin V. In Craig and Linke (18), the value for the stepping rate is referred to as the tethered diffusion rate.

*Values obtained from experimental data.

†Values obtained from balance conditions.

‡Values obtained by comparison of our calculations with the experimental data.

§Values obtained from simulations.

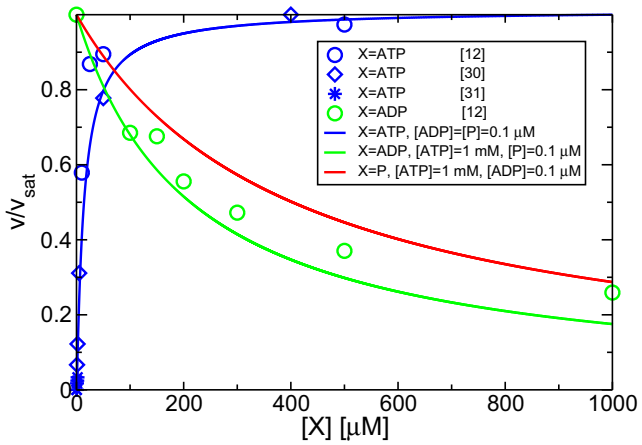

FIGURE 3 Stepping velocity v in units of the saturation velocity v_{sat} as a function of different nucleotide concentrations $[X]$. The experimental data are taken from the literature (12,30,31). (*Blue line*) Michaelis-Menten-like increase in velocity with increasing [ATP], for [ADP] = [P] = 0.1 μM, which agrees well with the experimental values measured by different groups (*blue symbols*). (*Green line*) Dependence on [ADP] at saturating concentration of ATP, [ATP] = 1 mM, and low phosphate concentration, [P] = 0.1 μM. An increasing [ADP] concentration reduces the stepping velocity, because the flux of the reverse dicycle $\mathcal{F}^-$ increases and, thus, reduces the dicycle excess flux $\Delta J(\mathcal{F}^+)$ as described by Eq. 6. We have rescaled the velocity by the saturating velocity because different experimental groups have reported different saturation velocities v_{sat}. Indeed, the myosin V construct studied in Baker et al. (12) was found to exhibit the saturating velocity v_{sat} = 550 nm/s, a value considerably higher than the value v_{sat} = 450 nm/s measured by other groups (1,7,11,30,34).

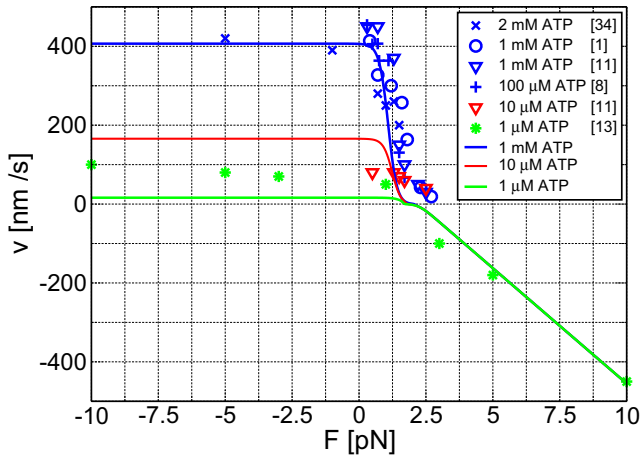

FIGURE 4 Stepping velocity v as a function of external load force F as calculated from the network in Fig. 2. We use the sign convention that positive values of F correspond to resisting forces. (*Solid lines*) Our theoretical results. (*Symbols*) Experimental data as obtained by several groups (1,8,11,13,34). These data were obtained for [ATP] $\geq$ 100 μM (*blue symbols*), [ATP] = 10 μM (*red triangles*), and [ATP] = 1 μM (*green asterisks*). (*Green*, *blue*, and *red lines*) Theoretical results for 1, 10, and 1000 μM ATP, respectively, with [ADP] = [P] = 0.1 μM. The theoretical value of the stall force is $F_s \simeq 2$ pN with a weak dependence on [ATP]. This value lies within the range -1.6 pN $\lesssim F_s \lesssim$ 2.5 pN as found experimentally. For forces $F < F_s$, the motor velocity depends on [ATP], while it becomes independent of [ATP] for $F >> F$, in agreement with the measurements in Gebhardt et al. (13).

resisting forces that do not exceed F_s, the behavior of myosin V qualitatively agrees with the behavior of kinesin (33). The motor velocity is rather insensitive to assisting forces and does not significantly change compared to the case of zero force (13,34). For superstall resisting forces, the step velocity turns out to be essentially independent of the concentration of ATP. Data for the motor velocity as obtained by several experimental groups is shown in Fig. 4, where we compare experimental findings with the results of our model calculations.

In the network description considered here, the velocity is governed by the competition between the mechanical slip or ratcheting cycle $\mathcal{M}$ and the chemomechanical forward cycle $\mathcal{F}$. This competition is strongly influenced by the binding rate of ATP. It can be understood by inspection of the branching points of the network, corresponding to the states 2 and 5 in Fig. 2. For the chemomechanical cycle $\mathcal{F}$ to be dominant, the transition rates ω_{25} and ω_{26} branching off to cycle $\mathcal{M}$ in state 2 have to be small compared to the rates within F. Because the ATP binding rate ω_{23} is large for saturating [ATP], the dicycle $\mathcal{F}^+$ is very robust for large [ATP]. Moreover, the dissipative cycle $\mathcal{E}$ supports this effect: For large [ATP] $\gtrsim$ 15 μM, the rapid rates of ATP binding and P release, κ_{56}[ATP] and κ_{62}, strongly drive the system toward $\mathcal{F}^+$, while the considerably slower rate κ_{25} of ADP dissociation leads from state 2 toward $\mathcal{M}$.

In state 5, the mechanical stepping rates $\omega_{55'}$ for the strongly bound state EE compete with ATP binding. This suggests that the ATP binding rate ω_{56} should decrease with increasing load force opposing the natural stepping direction of the motor. For switching between the two cycles $\mathcal{F}$ and $\mathcal{M}$, a minimal requirement is that the rates of ATP and ADP binding, ω_{56} and ω_{52}, in the enzymatic slip cycle $\mathcal{E}$ vanish in the limit of large resisting forces. This requirement is fulfilled by the force dependence as given by Eq. 11 with $F' = 1.6$ pN and $\chi_{56} = \chi_{52} = 4$, as mentioned before.

The force parameterization of the ADP binding rate takes two experimental observations into account. On the one hand, a decrease of the binding rate for single-headed constructs of Myosin V has been observed as a function of external load (10). It has been argued, on the other hand, that in double-headed molecules, internal strain weakens this effect for forces up to the stall force (5) which has been incorporated into the parameterization (11) via the force scale F'. For forces above stall, i.e., $F > F_s$, the occupation probability in the ratchet cycle rises, and the velocity is given by

$$v \simeq \ell \Delta J^{st}_{55'}, \tag{14}$$

while for $F < F_s$, we have

$$v \simeq \ell \Delta J^{st}_{34'}. \tag{15}$$

Fig. 4 shows calculations for three different concentrations of ATP, i.e., for [ATP] = 1, 100, and 1000 μM with the

concentrations of both ADP and P again fixed to 0.1 μM. As for the case of vanishing load force, the velocity depends, up to the stall force, on the concentration of ATP. For superstall forces, this behavior changes, and the velocity becomes independent of the ATP concentration.

For superstall forces, the ratchet or mechanical slip cycle $\mathcal{M}$ determines the behavior of the step velocity. The velocity increases roughly linearly with force, which reflects the fact that the mechanical transition rates $\omega_{55'}$ and $\omega_{5'5}$ given by Eqs. 9 and 10 are in the regime where the external force exceeds the barrier for performing a step in the EE state. The height of the potential barrier, U_{ba}, and the effective diffusion constant, D, are found to be $U_{ba} = 20\ k_BT$ and $D = 4.7 \times 10^2$(nm)^2/s. The parameters that we used for the force dependences are summarized in Table S1. A detailed view of the ratchet behavior is shown in Fig. S2, which compares our results with the data of Gebhardt et al. (13). The step velocity is shown as a function of [ATP] for $F = \pm 5$ and $F = \pm 10$ pN. For assisting forces, $F = -5$ and -10 pN, the motor velocity is similar to the force-free case, while the ratchet behavior is reproduced by our model for resisting forces as given by $F = 5$ and 10 pN.

For further extraction of motor parameters, we use the ratio of forward/backward steps as measured in Kad et al. (8) and shown in Fig. 5. For the network in Fig. 2, the average step ratio q, which is equal to the number of forward over the number of backward steps, is given by

$$q = \frac{P_3^{st}\omega_{34'} + P_5^{st}\omega_{55'}}{P_{4'}^{st}\omega_{4'3} + P_{5'}^{st}\omega_{5'5}}. \tag{16}$$

For small forces $F < F_s$, the motor behavior is dominated by the forward cycle $\mathcal{F}$. If we focus on this single cycle, the step ratio behaves as

$$q = \frac{P_3^{st}\omega_{34'}}{P_{4'}^{st}\omega_{4'3}} \approx 1 + \frac{\omega_{41}}{\omega_{4'3}} = 1 + \frac{\kappa_{41}}{\kappa_{4'3}\Phi_{4'3}(F)} \tag{17}$$

for small [P] and [ADP]. Note that, in the case of a single chemomechanical cycle, the stall force is reached only when the hydrolysis rate vanishes. This feature is a shortcoming of all unicycle models, as emphasized in Liepelt and Lipowsky (23). We use Eq. 17 to determine the backward stepping rate for $F = 0$, which is found to be $\kappa_{4'3} = 0.65\ s^{-1}$. Moreover, using the exponential force dependence of $\Phi_{4'3}(F)$ as given by Eq. 8, we obtain the parameter value $\theta = 0.65$.

The transition rates κ_{ij} and $\widehat{\kappa}_{ij}$ that have been determined experimentally and through our calculations as well as those obtained from the balance conditions are summarized in Table 2.

Run-length

To determine the run-length of the motor, we take the DD state as the most probable state for detachment, because the motor spends most of its dwell time between two subsequent steps in this state. The probability of detachment is then given by the probability to be in the state DD, P_1, times an unbinding rate ω_u, which leads to the run-length

$$\Delta x = \frac{v}{P_1\omega_u}. \tag{18}$$

The dependence of the run-length on the nucleotide concentrations is shown in Fig. 6 for unbinding rate $\omega_u = 0.4\ s^{-1}$. In Baker et al. (12), the experimentally determined run-length does not significantly change with increasing ATP concentration. In our theory, the run-length increases strongly for small [ATP] and then saturates above [ATP] $\simeq$ 40 μM.

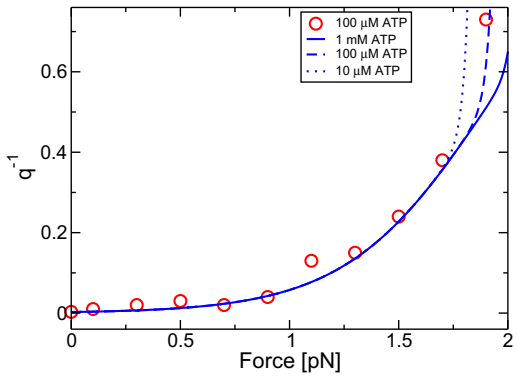

FIGURE 5 (Color online) Inverse step ratio q^{-1} of backward/forward steps as a function of load force F. (*Dotted*, *dashed*, and *solid lines*) Calculated using Eq. 16 for [ATP] = 10, 100, and 1000 μM, respectively, with constant [ADP] = [P] = 0.1 μM. For resisting forces that do not exceed F_s, the calculated step ratio is in good agreement with the experimental data (*circles*) as obtained in Kad et al. (8) for [ATP] = 100 μM. Note that this ratio is virtually independent of [ATP] for forces up to 1.6 pN.

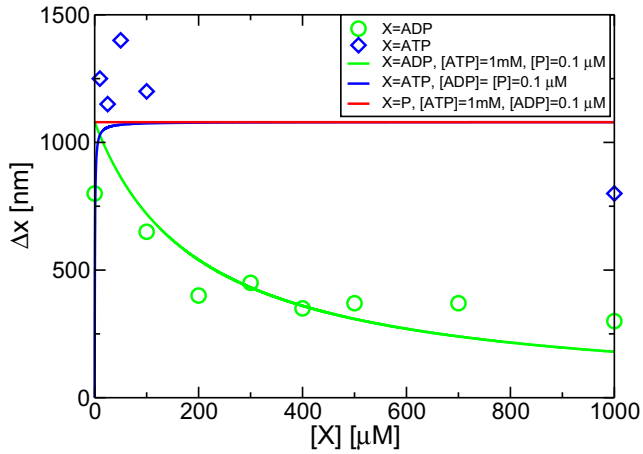

FIGURE 6 Run-length Δx as a function of different nucleotide concentrations [X] as explained in the inset. (*Solid curves*) Calculated using Eq. 18. (*All symbols*) Experimental data from Baker et al. (12).

Furthermore, the data in Baker et al. (12) showed a monotonic decrease in run-length with increasing ADP concentration, which is correctly reproduced by our calculation (see Fig. 6). These results have been obtained without the use of any additional fitting parameter apart from the unbinding rate $\omega_{u.}$

Because the motor state with bound ATP is more weakly bound to the filament, one would intuitively expect that unbinding occurs primarily from the states TD and DT. These latter states have, however, a relative low occupation probability, and unbinding from these states does not lead to a run-length that decreases with increasing ADP concentration as in Fig. 6. The unbinding rate $\omega_u = 0.4\ s^{-1}$ is smaller than the experimental values 1.5–20 s^{-1} as reported for single-headed myosin V with and without external load (32,35). For dimeric myosin, a dissociation rate of 0.004 s^{-1} has been reported in De La Cruz et al. (24). For substall forces and low concentrations of ADP and P, we find that the run-length does not depend on force, in agreement with the experimental observations in Clemen et al. (34).

DISCUSSION AND CONCLUDING REMARKS

We have studied the stepping properties of the molecular motor myosin V as a function of nucleotide concentration and external load in a quantitative way. Using a relatively simple network, we have described the motor's motion for forces both below and above the stall force. A network description that includes one main catalytic cycle reproduces both the velocity v and the run-length Δx as a function of nucleotide concentration in quantitative agreement with experimental findings, as shown in Figs. 3 and 6. The latter result does not depend on any additional fitting parameters apart from the unbinding rate $\omega_{u.}$

For small resisting forces F, both the motor velocity v (see Fig. 4) and the forward/backward step ratio q (see Fig. 5) stay roughly constant until they start to decrease strongly close to the stall force. The latter decrease reflects the decreasing probability of forward stepping via the chemomechanical cycle $\mathcal{F}$. For resisting forces that exceed the stall force, our network description captures the ratcheting behavior of the motor, as shown in Fig. 4. The forced backward stepping arises from the mechanical cycle $\mathcal{M}$ with step rates that have been derived from a discretized Fokker-Planck equation (see Eqs. 9 and 10). Switching the operation mode of the motor from the chemomechanical cycle $\mathcal{F}$ to the mechanical ratchet cycle $\mathcal{M}$ for large load forces F should be useful if myosin V and kinesin are attached to the same intracellular cargo particle as observed experimentally in Ali et al. (36) and considered theoretically in Berger et al. (37).

In these latter studies, the myosins and kinesins moved along the same filament. If the myosins are in contact with actin filaments whereas the kinesins move along microtubules as discussed, e.g., in Holzbaur and Goldman (38), the switching from the chemomechanical cycle $\mathcal{F}$ to the mechanical ratchet cycle $\mathcal{M}$ allows the myosins to stay in touch with the actin filaments even if the kinesins pull in the opposite direction and generate forces of the order of their stall force, which is ~7 pN.

The competition between the chemomechanical cycle $\mathcal{F}$ and the mechanical cycle $\mathcal{M}$ essentially depends on the binding rates of ATP and ADP in the enzymatic cycle $\mathcal{E}$. Both rates decrease for a high load force, while the other chemical rates need not depend on force. For substall forces, the force dependence of ADP binding and release as well as of ATP binding is believed to be weak for dimeric myosin V (5,32,35). The decrease of the binding rates for superstall forces could arise from a deformation of the molecule. For this regime, an inhibition of the powerstroke of myosin V has been observed, which can lead to the decline of its catalytic function. A possible mechanism is provided by a partial closure of the nucleotide-binding pocket of the leading head, when the motor molecule experiences superstall load forces. It remains to be seen whether such a molecular mechanism can be corroborated by further experimental studies.

SUPPORTING MATERIAL

Six sections with 27 equations, two figures, and one table are available at http://www.biophysj.org/biophysj/supplemental/S0006-3495(11)00202-5.

REFERENCES

1. Mehta, A. D., R. S. Rock, …, R. E. Cheney. 1999. Myosin-V is a processive actin-based motor. *Nature.* 400:590–593.
2. Sakamoto, T., M. R. Webb, …, J. R. Sellers. 2008. Direct observation of the mechanochemical coupling in myosin Va during processive movement. *Nature.* 455:128–132.
3. Yildiz, A., J. N. Forkey, …, P. R. Selvin. 2003. Myosin V walks hand-over-hand: single fluorophore imaging with 1.5-nm localization. *Science.* 300:2061–2065.
4. Veigel, C., F. Wang, …, J. E. Molloy. 2002. The gated gait of the processive molecular motor, myosin V. *Nat. Cell Biol.* 4:59–65.
5. Veigel, C., S. Schmitz, …, J. R. Sellers. 2005. Load-dependent kinetics of myosin-V can explain its high processivity. *Nat. Cell Biol.* 7: 861–869.
6. Shiroguchi, K., and K. Kinosita, Jr. 2007. Myosin V walks by lever action and Brownian motion. *Science.* 316:1208–1212.
7. Rief, M., R. S. Rock, …, J. A. Spudich. 2000. Myosin-V stepping kinetics: a molecular model for processivity. *Proc. Natl. Acad. Sci. USA.* 97:9482–9486.
8. Kad, N. M., K. M. Trybus, and D. M. Warshaw. 2008. Load and Pi control flux through the branched kinetic cycle of myosin V. *J. Biol. Chem.* 283:17477–17484.
9. Rosenfeld, S. S., and H. L. Sweeney. 2004. A model of myosin V processivity. *J. Biol. Chem.* 279:40100–40111.
10. Oguchi, Y., S. V. Mikhailenko, …, S. Ishiwata. 2008. Load-dependent ADP binding to myosins V and VI: implications for subunit coordination and function. *Proc. Natl. Acad. Sci. USA.* 105:7714–7719.
11. Uemura, S., H. Higuchi, …, S. Ishiwata. 2004. Mechanochemical coupling of two substeps in a single myosin V motor. *Nat. Struct. Mol. Biol.* 11:877–883.

12. Baker, J. E., E. B. Krementsova, …, D. M. Warshaw. 2004. Myosin V processivity: multiple kinetic pathways for head-to-head coordination. *Proc. Natl. Acad. Sci. USA.* 101:5542–5546.

13. Gebhardt, J. C., A. E.-M. Clemen, …, M. Rief. 2006. Myosin-V is a mechanical ratchet. *Proc. Natl. Acad. Sci. USA.* 103:8680–8685.

14. Skau, K. I., R. B. Hoyle, and M. S. Turner. 2006. A kinetic model describing the processivity of myosin-V. *Biophys. J.* 91:2475–2489.

15. Vilfan, A. 2005. Elastic lever-arm model for myosin V. *Biophys. J.* 88:3792–3805.

16. Liao, J.-C., J. A. Spudich, …, S. L. Delp. 2007. Extending the absorbing boundary method to fit dwell-time distributions of molecular motors with complex kinetic pathways. *Proc. Natl. Acad. Sci. USA.* 104:3171–3176.

17. Schmiedl, T., and U. Seifert. 2008. Efficiency of molecular motors at maximum power. *Europhys. Lett.* 83:30005.

18. Craig, E. M., and H. Linke. 2009. Mechanochemical model for myosin V. *Proc. Natl. Acad. Sci. USA.* 106:18261–18266.

19. Cappello, G., P. Pierobon, …, J. Prost. 2007. Myosin V stepping mechanism. *Proc. Natl. Acad. Sci. USA.* 104:15328–15333.

20. Kolomeisky, A. B., and M. E. Fisher. 2003. A simple kinetic model describes the processivity of myosin-v. *Biophys. J.* 84:1642–1650.

21. Tsygankov, D., and M. E. Fisher. 2007. Mechanoenzymes under superstall and large assisting loads reveal structural features. *Proc. Natl. Acad. Sci. USA.* 104:19321–19326.

22. Lipowsky, R., S. Liepelt, and A. Valleriani. 2009. Energy conversion by molecular motors coupled to nucleotide hydrolysis. *J. Stat. Phys.* 135:951–975.

23. Liepelt, S., and R. Lipowsky. 2007. Kinesin's network of chemomechanical motor cycles. *Phys. Rev. Lett.* 98:258102.

24. De La Cruz, E. M., A. L. Wells, …, H. L. Sweeney. 1999. The kinetic mechanism of myosin V. *Proc. Natl. Acad. Sci. USA.* 96:13726–13731.

25. Dunn, A. R., and J. A. Spudich. 2007. Dynamics of the unbound head during myosin V processive translocation. *Nat. Struct. Mol. Biol.* 14:246–248.

26. Astumian, R. D. 2010. Thermodynamics and kinetics of molecular motors. *Biophys. J.* 98:2401–2409.

27. Liepelt, S., and R. Lipowsky. 2007. Steady-state balance conditions for molecular motor cycles and stochastic nonequilibrium processes. *EPL.* 77:50002.

28. Robblee, J. P., W. Cao, …, E. M. De La Cruz. 2005. Thermodynamics of nucleotide binding to actomyosin V and VI: a positive heat capacity change accompanies strong ADP binding. *Biochemistry.* 44:10238–10249.

29. Friedman, A. L., M. A. Geeves, …, J. A. Spudich. 1998. Kinetic characterization of myosin head fragments with long-lived myosin.ATP states. *Biochemistry.* 37:9679–9687.

30. Forkey, J. N., M. E. Quinlan, …, Y. E. Goldman. 2003. Three-dimensional structural dynamics of myosin V by single-molecule fluorescence polarization. *Nature.* 422:399–404.

31. Komori, Y., A. H. Iwane, and T. Yanagida. 2007. Myosin-V makes two Brownian 90° rotations per 36-nm step. *Nat. Struct. Mol. Biol.* 14: 968–973.

32. Purcell, T. J., H. L. Sweeney, and J. A. Spudich. 2005. A force-dependent state controls the coordination of processive myosin V. *Proc. Natl. Acad. Sci. USA.* 102:13873–13878.

33. Carter, N. J., and R. A. Cross. 2005. Mechanics of the kinesin step. *Nature.* 435:308–312.

34. Clemen, A. E.-M., M. Vilfan, …, M. Rief. 2005. Force-dependent stepping kinetics of myosin-V. *Biophys. J.* 88:4402–4410.

35. Sellers, J. R., and C. Veigel. 2010. Direct observation of the myosin-Va power stroke and its reversal. *Nat. Struct. Mol. Biol.* 17:590–595.

36. Ali, M. Y., H. Lu, …, K. M. Trybus. 2008. Myosin V and kinesin act as tethers to enhance each others' processivity. *Proc. Natl. Acad. Sci. USA.* 105:4691–4696.

37. Berger, F., M. J. I. Müller, and R. Lipowsky. 2009. Enhancement of the processivity of kinesin-transported cargo by myosin V. *EPL.* 87:28002.

38. Holzbaur, E. L. F., and Y. E. Goldman. 2010. Coordination of molecular motors: from in vitro assays to intracellular dynamics. *Curr. Opin. Cell Biol.* 22:4–13.